



Redox-dependent loss of flavin by mitochondria complex I is different in brain and heart

Belem Yoval-Sánchez^a, Fariha Ansari^a, Joel James^b, Zoya Niatsets kaya^c, Sergey Sosunov^c, Peter Filipenko^g, Irina G. Tikhonova^d, Vadim Ten^c, Ilka Wittig^{e,f}, Ruslan Rafikov^b, Alexander Galkin^{a,*}

^a Feil Family Brain and Mind Research Institute, Weill Cornell Medicine, 407 East 61st Street, New York, NY, 10065, USA

^b Division of Endocrinology, Department of Medicine, University of Arizona College of Medicine, Tucson, AZ, USA

^c Department of Pediatrics, Rutgers-Robert Wood Johnson Medical School, New Brunswick, NJ, 08901, USA

^d School of Pharmacy, Medical Biology, Centre, Queen's University Belfast, Belfast, BT9 7BL, United Kingdom

^e Functional Proteomics, Cardiovascular Physiology, Goethe University, 60590, Frankfurt am Main, Germany

^f German Center for Cardiovascular Research (DZHK), Partner site RheinMain, Frankfurt, Germany

^g Department of Biochemistry, Weill Cornell Medical College, Cornell University, New York, NY, 10021, USA

ARTICLE INFO

Keywords:

Mitochondrial complex I
Flavin mononucleotide
Reverse electron transfer
Heart
Brain
Tissue-specificity
Isoforms
Stroke
Cardiac infarction

ABSTRACT

Pathologies associated with tissue ischemia/reperfusion (I/R) in highly metabolizing organs such as the brain and heart are leading causes of death and disability in humans. Molecular mechanisms underlying mitochondrial dysfunction during acute injury in I/R are tissue-specific, but their details are not completely understood. A metabolic shift and accumulation of substrates of reverse electron transfer (RET) such as succinate are observed in tissue ischemia, making mitochondrial complex I of the respiratory chain (NADH:ubiquinone oxidoreductase) the most vulnerable enzyme to the following reperfusion. It has been shown that brain complex I is predisposed to losing its flavin mononucleotide (FMN) cofactor when maintained in the reduced state in conditions of RET both *in vitro* and *in vivo*. Here we investigated the process of redox-dependent dissociation of FMN from mitochondrial complex I in brain and heart mitochondria. In contrast to the brain enzyme, cardiac complex I does not lose FMN when reduced in RET conditions. We proposed that the different kinetics of FMN loss during RET is due to the presence of brain-specific long 50 kDa isoform of the NDUFV3 subunit of complex I, which is absent in the heart where only the canonical 10 kDa short isoform is found. Our simulation studies suggest that the long NDUFV3 isoform can reach toward the FMN binding pocket and affect the nucleotide affinity to the apoenzyme. For the first time, we demonstrated a potential functional role of tissue-specific isoforms of complex I, providing the distinct molecular mechanism of I/R-induced mitochondrial impairment in cardiac and cerebral tissues. By combining functional studies of intact complex I and molecular structure simulations, we defined the critical difference between the brain and heart enzyme and suggested insights into the redox-dependent inactivation mechanisms of complex I during I/R injury in both tissues.

1. Introduction

Ischemia-reperfusion (I/R) injury takes place when blood supply returns to tissue after a period of ischemia or lack of oxygen. The most common manifestation of I/R injury in humans can be found in a cohort of cardiovascular diseases, such as ischemic stroke, neonatal hypoxic-ischemic encephalopathy, heart infarction or cardiac arrest. Together, they are a major cause of death worldwide, with over 17 million people dying of these conditions each year and around \$363.4 billion of life cost

in the USA [1].

Initially, tissue ischemia or loss of blood flow results in a fast drop in oxygen level, leading to the deceleration of mitochondrial oxidative phosphorylation and a dramatic depletion of high-energy phosphates (triphosphate nucleosides and creatine phosphate). This also changes the tissue metabolic landscape towards accumulation of certain catabolic metabolites and intermediate substrates of respiration (*i.e.*, reducing equivalents). Following reperfusion, there is a transient burst of respiration and restoration of the mitochondrial energy-producing function. Reoxygenation, however, triggers mechanisms of reperfusion

* Corresponding author.

E-mail address: alg2057@med.cornell.edu (A. Galkin).

List of abbreviations

BSA	bovine serum albumin
DDM	n-dodecyl- β -D-malteseide;
DLD	dihydrolipoyl dehydrogenase
EGTA	ethylene glycol-bis(β -aminoethyl ether)-N,N,N',N'-tetraacetic acid
FAD	flavin adenine dinucleotide;
FMN	flavin mononucleotide;
HAR	hexaammineruthenium chloride (II)
hrCN	electrophoresis, high resolution clear native electrophoresis
I/R	ischemia/reperfusion
KGDHC	α -ketoglutarate dehydrogenase complex
MSE	mannitol/sucrose/EGTA medium
Q ₁	ubiquinone-1, 2,3-Dimethoxy-5-methyl-6-(3-methyl-2-butenyl)-1,4-benzoquinone
RET	reverse electron transfer
SDS	sodium dodecyl sulfate

injury and oxidative stress, which augment damage to mitochondria [2–5]. Although anaerobic formation of succinic acid has been known since pioneering studies of the TCA cycle in the 1930s [6–8], the process of ischemic accumulation of succinate gained recent attention in light of its role in the development of I/R tissue injury [9–16]. We and others showed that oxidation of elevated levels of succinate during reperfusion/reoxygenation of post-ischemic tissue leads to conditions of reverse electron transfer (RET) [11,17,18]. Under RET conditions, electrons from succinate are directed to ubiquinone, reducing it to ubiquinol. Oxidation of the ubiquinol pool is coupled with proton translocation across the membrane by complexes III and IV. In the presence of a proton-motive force, a small fraction of the electrons from ubiquinol can be directed upstream to complex I, maintaining most of the redox centers of the enzyme (FeS clusters and FMN) in the reduced form. This is a reversal of the NADH:ubiquinone oxidoreduction of complex I, and given the availability of NAD⁺, it is possible to demonstrate reduction of the nucleotide *in vitro* in coupled preparations of mitochondria or sub-mitochondrial particles [19–25]. In intact mitochondria, steady-state oxidation of RET-substrates provides a high ubiquinol/ubiquinone ratio and builds up a sufficient proton-motive force to support complete reduction of NAD(P)⁺ in the matrix. After depletion of the matrix NAD(P)⁺ pool, there would be no RET (succinate:NAD⁺ oxidoreduction) as originally defined by Chance [19]. In the absence of the oxidized nucleotide, FMN of complex I is maintained in the reduced state. Previously, we suggested the term RET-like conditions to describe this process of oxidation of succinate by coupled intact mitochondria in steady-state [5,18,26]. When matrix nucleotides are fully reduced, the only electron acceptor for RET-linked electron flux at complex I is molecular oxygen, which is reduced to superoxide by the flavin. In these conditions when all redox centers of complex I are reduced, the rate of RET via complex I represents a ROS-generating “leak” of electrons to oxygen [27]. In the absence of inhibitors, when intact mitochondria oxidize succinate in RET-like conditions, ROS generation is the highest, representing 2–5% of the total electron flux [18,28–31]. Because of its high contribution to ROS production, mitochondrial RET emerged as a potential area of great pathophysiological importance [11,17,18,32–34]. Recently, we demonstrated that over-reduction of complex I in brain mitochondria in RET-like conditions results in dissociation of the natural flavin cofactor from the enzyme *in vitro* [26] and in *in vivo* models of brain I/R [18,35]. At the same time, the process of ROS generation via succinate-supported RET during heart I/R has been shown to play a significant role in the development of cardiac tissue injury [11,14]. While it is generally accepted that there are

tissue-specific alterations in mitochondrial content, stoichiometry of respiratory chain complexes and activity of individual enzymes, the extent of differences in the process of RET in different tissues is not clear. Therefore, the aim of this study was to compare the mechanism of redox-dependent flavin loss between brain and heart mitochondria.

In the present manuscript, we assessed RET-induced dissociation of FMN from complex I in brain and heart mitochondria using a novel approach for quantitative analysis of flavin content of the enzyme. We compared kinetic parameters of FMN loss by the enzyme from both tissues. We also confirmed that the brain and heart enzyme subunit composition is different, suggesting for the first time the functional role of tissue-specific isoforms of mitochondrial complex I and providing the distinct molecular mechanism of I/R-induced mitochondrial impairment in cardiac and cerebral tissue.

2. Materials and methods

2.1. Sources of chemicals

Chemicals were purchased from Sigma: bovine serum albumin (BSA) essentially fatty acid free (#A6003), DDM (#D4641), hexaammineruthenium (III) chloride (#262005), horseradish peroxidase (#P8250), mannitol (#63559), NADH (#N8129), Q₁ (#C7956), SOD (#S9697), sucrose (#S7903), and triphenyl-tetrazolium chloride (#T8877). 3–12% acrylamide gradient gel (#BN1001BOX), Amplex UltraRed (#A36006), NativeMark™ unstained protein standards (#LC0725), PageBlue Protein Staining Solution (#24620), and Pierce BCA protein assay kit (#23225) were from Thermo Fisher Scientific. Alamethicin (#11425) and atpenin A5 (#11898) were from Cayman Chemical.

2.1.1. Isolation of intact brain mitochondria for *in vitro* studies

Intact brain mitochondria were isolated from C57BL6/J mice by differential centrifugation with digitonin treatment [18,26]. Intact heart mitochondria were isolated in accordance to Ref. [36].

2.1.2. Measurement of H₂O₂ release

Mitochondrial respiration and H₂O₂ release were measured using a high-resolution respirometer (Oroboros Oxygraph-2k®) equipped with two-channel fluorescence optical setup to use with the Amplex UltraRed and horseradish peroxidase assay [28,37]. In brief, mitochondria (0.05–0.2 mg/ml) were added to 2 ml of assay medium composed of 125 mM KCl, 0.2 mM EGTA, 20 mM HEPES-Tris, 4 mM KH₂PO₄, pH 7.4, 2 mM MgCl₂, 1 mg/ml BSA, 10 μ M Amplex UltraRed, 10 U/ml SOD and 4 U/ml horseradish peroxidase at 37 °C. To initiate respiration in RET-like conditions, 5 mM succinate and 1 mM glutamate were used. Respiration was fully sensitive to 1 mM cyanide or 0.2 μ M atpenin. The H₂O₂ assays were calibrated by the addition of standard aliquots of freshly prepared H₂O₂ from a stock solution of known concentration ($\epsilon_{240nm} = 46.3 \text{ M}^{-1} \text{ cm}^{-1}$).

2.1.3. Flavin fluorescence measurements in mitochondrial fragments

Permeabilized mitochondrial fragments (50 and 20 μ g protein/ml of the brain and heart, respectively) were preincubated at 25 °C in the standard assay mixture (pH 8.5) supplemented with 1 mM cyanide, 40 μ g/ml alamethicin, and 200 μ M NADH. The time course of flavin fluorescence during forward electron transfer was monitored with the Hitachi F-7000 fluorospectrophotometer ($\lambda_{exc/em} = 450/525 \text{ nm}$).

2.1.4. Measurement of mitochondrial activities

Activities of mitochondrial membranes were measured spectrophotometrically using the Molecular Devices SpectraMax M2 plate reader in 0.2 ml of assay buffer (125 mM KCl, 20 mM HEPES-Tris, 0.2 mM EGTA, pH 7.4 or 8.5) at 25 °C [18,35].

NADH-dependent activities of complex I were assayed as oxidation of 0.2 mM NADH at 340 nm ($\epsilon_{340nm} = 6.22 \text{ mM}^{-1} \text{ cm}^{-1}$) in assay buffer supplemented with 1 mg/ml BSA, 40 μ g/ml alamethicin and 1 mM KCN

(NADH media). NADH:Q reductase was measured in NADH media containing 1 mg/ml BSA, 60 μ M ubiquinone, and 5–20 μ g protein per well. NADH:HAR reductase was assayed in NADH media containing 1 mM HAR and 5–20 μ g protein per well.

2.1.5. High resolution clear native electrophoresis, flavin fluorescence scanning, and Western blot analysis

Sample solubilization with DDM and running conditions for high resolution clear native (hrCN) electrophoresis of mitochondrial membranes and tissues was essentially done as described [38,39]. Gels were analyzed either for complex I in-gel activity, stained with Coomassie or scanned for flavin fluorescence in a Typhoon 9000 gel scanner (GE) using a 473 nm laser and BPB1 filter (530 nm maximum, 20 nm band-pass). For the in-gel activity assay of complex I, gels were placed in 10 mL of buffer containing 5 mM Tris-HCl pH 7.4, 0.2 mM EDTA, and 3 mM nitro blue tetrazolium. 150 μ M NADH was added to the reaction and after 3–5 min, gels were transferred to a fixing solution of 50% methanol and 10% acetic acid [38]. PageBlue Protein Staining Solution was used for staining protein bands. For the Western Blot, we used an antibody against the S8 subunit of the mitochondrial membrane respiratory chain NADH dehydrogenase (complex I) (Rabbit monoclonal NDUF58 - C-terminal; Abcam Cat# ab180183; dilution 1:2000; 2% milk; 2h at room temperature). Blot images were obtained using Fluorchem M Western Imaging System (Protein Simple, San Jose, CA) [39].

2.1.6. Complexome profiling and MS/MS analysis

Liquid chromatography/mass spectrometry (LC/MS) was performed on a Thermo Scientific™ Q Exactive Plus equipped with an ultra-high performance liquid chromatography unit (Thermo Scientific Dionex Ultimate 3000) and a Nanospray Flex Ion-Source (Thermo Scientific) as described previously [18]. For data analysis, MaxQuant (13), NOVA [40] and Excel (Microsoft Office 2013) were used. Proteins were identified by using the mouse reference proteome database UniProtKB. Acetylation (+42.01) at the N-terminus and oxidation of methionine (+15.99) were selected as variable modifications, and carbamidomethylation (+57.02) was selected as fixed modification on cysteines. The enzyme specificity was set to Trypsin. False discovery rate (FDR) for the identification protein and peptides was 1%. Heatmap of proteins represents the abundance normalized to maximum appearance in a native electrophoresis lane.

2.1.7. Computational analysis

Due to the absence of the complete X-ray structure for NDUFV3 long (NDUFV3-L) isoform, we utilized the homology modeling module of YASARA (Yet Another Scientific Artificial Reality Application) [41]. YASARA includes a full homology modeling package that completely automates steps from the amino acid sequence input, alignment, building loops, stereochemistry optimization, and homology model validation. The homology modeling parameter settings are as follows: the modeling speed was set to slow, the number of PSI-BLAST iterations in template search was set to 3, the maximum allowed PSI-BLAST E-value was 0.1, the maximum number of the templates to be used was 3, the maximum number of templates with the same sequence was 1, maximum oligomerization state was 4, a maximum number of alignment variations per template was 5, a maximum number of conformations tried per loop was 50 and the maximum number of residues added to the termini was 10. In summary, the NDUFV3-L homology model was developed using the following protocol: the sequence was split into three for N-, C-terminus region and middle domain, a PSI-BLAST integrated into YASARA was used to identify the closest templates in the PDB for each part of the protein. Three templates were identified (PDB codes 6ZKD [42], 4V6W [43], 7CEE [44]). We used BLAST to retrieve homologous sequences, create a multiple sequence alignment, and enter the sequences into a “discrimination of secondary structure class” prediction algorithm. The side chains were added and optimized in the next step, and all modeled parts were combined and

subjected to an automated module in YASARA, which combined the steepest descent and simulated annealing minimization. The backbone atoms of the aligned residues were kept fixed. Finally, an unrestrained, simulated annealing minimization with water was performed on the entire model, automated by YASARA. Subsequently, the resulting structure of full-length NDUFV3-L was used for protein docking to complex I subunits. The NDUFV1, NDUFV2, and NDUF51 subunits were separated from complex I (PDB ID: 6G2J [45]), and a PDB file of these 3 subunits together was generated. Additionally, a PDB file of N-domain NDUFV3-L was generated after truncating at Gln421. Following this, energy minimization was done in YASARA. The PDBs were then submitted to the ClusPro server for protein-protein docking to understand how NDUFV3-L interacts with the NDUFV1, NDUFV2, and NDUF51 subunits of complex I. The ClusPro server performs the following computational steps: first, a rigid-body docking with billions of conformations using PIPER [46,47] is performed. PIPER is a Fast Fourier Transform (FFT) approach to protein-protein docking and is useful in constructing the structure and predicting the interactions of large multi-domain proteins. The second step consists of a root-mean-square deviation (RMSD) clustering and selecting the 1000 lowest-energy structures. Finally, energy minimization and refinement of selected structures are done. A detailed procedure of the ClusPro docking process is described previously [46,48–50]. Visualization and image processing of the docked complexes with the top 10 balanced coefficients was then performed in YASARA. The first docked complex that showed a sterically possible conformation (second highest balanced coefficient) was then used for further analysis and imaging.

2.1.8. Statistical analysis

Gel fluorescence scans were analyzed using ImageLab software (Biorad). Region of interest (ROI) amplitude measurements were placed over the fluorescence band and the intensity was calculated with background subtracted. Data analysis was performed using Microcal Origin (version 8Pro). All data are mean \pm SEM unless otherwise specified. Statistically significant differences are indicated (*) when $p < 0.05$. A two-tailed *t*-test or Mann-Whitney test was used to analyze intergroup differences between two groups. One-way ANOVA and Dunnett’s test were used to compare groups after and before treatment. For other comparisons between groups, multiple *t*-tests with FDR correction for multiple comparisons were used.

3. Results

3.1. Effect of forward and reverse electron transfer on the activity of brain and heart mitochondrial complex I

Complex I from mitochondria and bacteria is susceptible to reductive inactivation when directly reduced by NADH in the forward mode in alkaline media [51–53]. When reduced by NADH, FMN dissociates from the bovine heart enzyme with a half-time of inactivation of around 20 min [53]. The process of reductive inactivation is faster for the mouse enzyme when fragmented mitochondria are incubated in the presence of NADH in mildly alkaline conditions (pH 8.5) (Fig. 1). Exogenously added FMN recovered complex I activity indicating reversibility of FMN dissociation.

Previously, using mouse intact brain mitochondria we demonstrated that the rate of H₂O₂ release when mitochondria are oxidizing succinate declines with time due to complex I inactivation [18,26]. We examined if H₂O₂ release rate in succinate-supported RET-like conditions also declines in intact heart mitochondria. First, we compared respiratory and H₂O₂ release activities of brain and heart mitochondria. Table 1 shows the quantitative characteristics of mitochondrial respiration and H₂O₂ release in RET-like conditions measured at ambient oxygen concentration (200 μ M O₂ at 37 °C). We found that the cardiac preparation demonstrated significantly higher respiration per mg of protein in comparison with intact brain mitochondria. The respiratory control

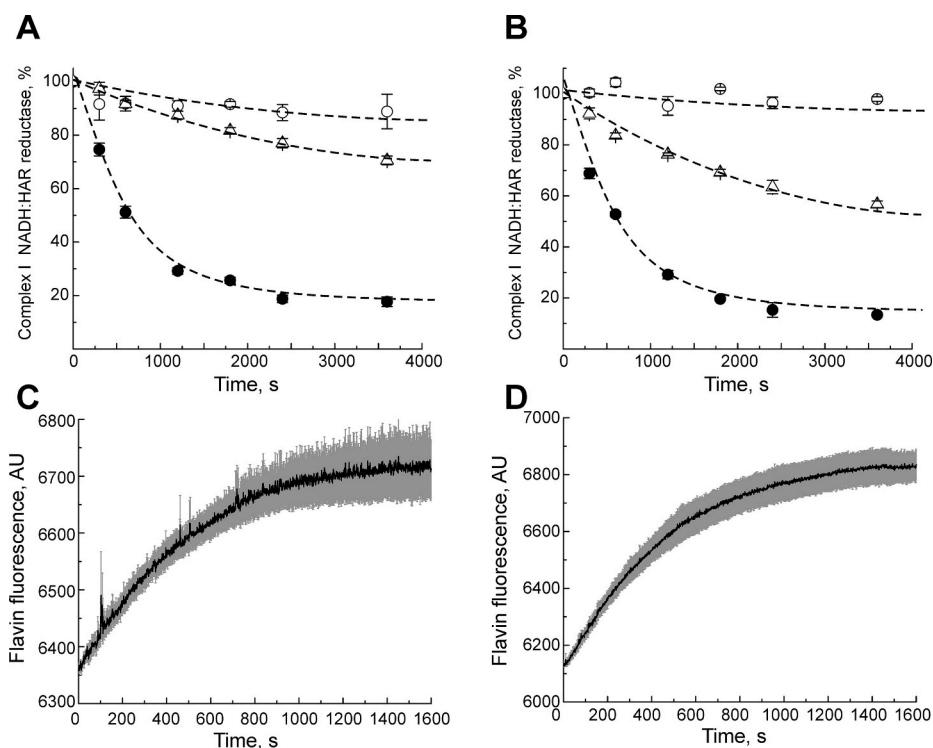


Fig. 1. NADH-induced reductive inactivation of brain and heart mitochondrial complex I. (A, B) Fragments of mitochondrial membranes (50 and 20 μg protein/ml of the brain (A) and heart (B), respectively) were preincubated at 25 °C in the standard assay mixture (pH 8.5) supplemented with 1 mM cyanide, 40 μg/ml alamethicin, with or without 200 μM NADH (solid and empty circles, respectively). Aliquots were taken and the rate of NADH oxidation was initiated by the addition of 1 mM HAR. 20 μM FMN was added to the complex I activity assay after NADH-induced inactivation (triangles). 100% corresponds to a specific activity of 0.96 ± 0.01 and 3.17 ± 0.19 μmol NADH × min⁻¹ × mg⁻¹ for the brain and heart, respectively. Results show mean ± SD (n = 3). (C, D) The time course of flavin fluorescence ($\lambda_{exc/em} = 450/525$ nm) was monitored simultaneously in similar conditions as in panels A and B. Averaged time course of fluorescence intensity is shown for the brain (C) and heart (D) mitochondrial fragments. Grey error bars represent SEM based on triplicate measurements.

Table 1

Respiration activities and H₂O₂ release by coupled mouse brain and heart mitochondria during oxidation of succinate in RET-like conditions.

	Respiration nmol O ₂ × min ⁻¹ × mg ⁻¹		Release of H ₂ O ₂ ^a nmol H ₂ O ₂ × min ⁻¹ × mg ⁻¹	
	Brain	Heart	Brain	Heart
State 2 (non-phosphorylating)	50 ± 5	164 ± 1	1.16 ± 0.05	3.43 ± 0.20
State 3(+0.2 mM ADP)	232 ± 14	345 ± 23	0.19 ± 0.023	n.d.

^a Measured simultaneously, as described in the Materials and Methods section, in 125 mM KCl, 0.2 mM EGTA, 20 mM HEPES-Tris, 4 mM KH₂PO₄, pH 7.4, 2 mM MgCl₂, 1 mg/ml BSA, 10 μM Amplex UltraRed, 4 U/ml horseradish peroxidase, 10 U/ml SOD, 5 mM succinate and 1 mM glutamate at 37 °C using 0.05–0.2 mg of protein/ml. Values are given as mean ± SEM (n = 3–4).

ratio on NADH-generating substrates such as malate/pyruvate/glutamate was 8.5 ± 3.0 and 7.9 ± 0.6 for the brain and heart mitochondria, respectively, indicating a similar degree of coupling in both preparations. RET-like conditions provided the greatest rate in H₂O₂ release equivalent to approximately 2.3% and 4.7% of total oxygen consumption in the brain and heart mitochondria, respectively, indicating significantly higher ROS generation capacity in the cardiac preparation. Fig. 2 demonstrates the time course of H₂O₂ release during oxidation of succinate by brain (Fig. 2A, C) and heart (Fig. 2B, D) intact mitochondria. RET-induced H₂O₂ release is shown as a fluorescence intensity increase in time due to the formation of resorufin as a product of the oxidation of Amplex UltraRed by H₂O₂ (Fig. 2A and B). This signal was then differentiated by the DatLab software and can be plotted directly as absolute rates of H₂O₂ release (nM/min) during the time course of the assay. After reaching a maximal rate of H₂O₂ release, a gradual exponential decline in the rate with a half-time of exponential decay of around 4.3 and 28.0 min was observed in the brain and heart, respectively (Fig. 2C and D, red fitting line).

We also assessed the physiological activity of mitochondrial complex I in mitochondria oxidizing succinate (Fig. 2E and F). During incubation

of the mitochondrial suspension in RET-like conditions, small aliquots were taken and the NADH:Q reductase activity of the enzyme was further assayed after membrane permeabilization. We found that specific complex I activity decreases in parallel with the decline of H₂O₂ release rate (Fig. 2E), in agreement with our previously published data [18]. Complex I inactivation was not observed in the heart mitochondria oxidizing succinate (Fig. 2F) indicating that enzyme from cardiac tissue is less affected by RET-like conditions.

3.2. Direct detection of mitochondrial complex I FMN

While the data shown in Figs. 1 and 2 suggest that dissociation of FMN was the cause of the NADH-induced inactivation of complex I in the brain, the FMN content of complex I before and after redox-dependent inactivation has never been directly determined. In the past, we performed analysis of non-covalently bound FMN content in deproteinized extracts of brain mitochondria preparations after incubation in RET-like conditions [18]. It strongly suggested that the mechanism of inactivation of the brain enzyme is in fact redox-dependent dissociation of tightly bound complex I flavin. In order to directly identify the mechanism of complex I inactivation, we developed a method to accurately determine only complex I-associated FMN in mitochondrial preparations [39]. A typical Coomassie-stained hrCN PAGE gel of DDM-solubilized intact mitochondria from the brain and heart is shown in Fig. 3A, lanes 2. The complex I band was specifically stained by an “in-gel” NADH:nitro tetrazolium reaction catalyzed by the enzyme (Fig. 3A, lanes 3). Flavin of complex I, however, was not detected in the native gel because enzyme-bound FMN fluorescence is quenched in the intact enzyme [54,55]. The fluorescence signal from complex I FMN could only be revealed after denaturing the complex. Treatment of the gel with 20% SDS led to the appearance of a strong flavin fluorescence signal as a single band corresponding to the position of complex I (~850 kDa) (Fig. 3A, lanes 4, 5). The position of the complex I band was also confirmed by a Western blot (Fig. 3A, lanes 6).

After denaturation of the native protein by SDS [39], we observed two major flavin-containing bands corresponding to mitochondrial α-ketoglutarate dehydrogenase (αKGDHC) and complex I (Fig. 3A, lanes

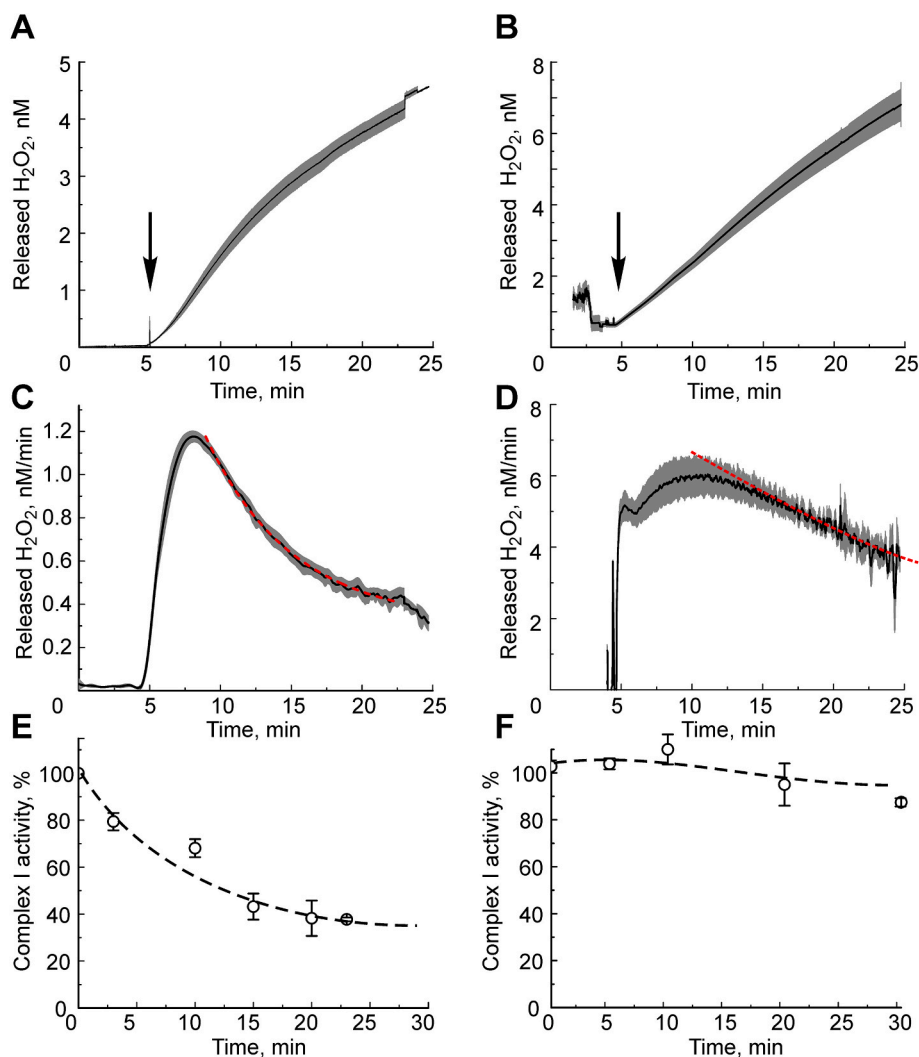


Fig. 2. Effect of succinate oxidation in RET-like conditions by preparations of brain (left) and heart (right) mitochondria on H₂O₂ release rates and complex I physiological activity. The reaction was started by addition of 5 mM succinate and 1 mM glutamate to the medium composed of 125 mM KCl, 0.2 mM EGTA, 20 mM HEPES-Tris (pH 7.4), 4 mM KH₂PO₄, 2 mM MgCl₂, 1 mg/ml BSA, 10 μM Amplex UltraRed, 4 U/ml horseradish peroxidase and 10 U/ml SOD at 37 °C. (A, B) Averaged time course of H₂O₂ increase in the assay (as resorufin fluorescence) by brain (100 μg/ml, A) and heart (50 μg/ml, B) mitochondria. Substrate addition is shown by an arrow. (C, D) The rate of H₂O₂ release (derivative of the raw signal) for brain and heart mitochondria, respectively. Fitting of the exponential decay function is shown by red dashed lines. (E, F) Effect of incubation of intact brain mitochondria in RET-like conditions on NADH:Q₁ reductase activity. Brain (0.1 mg of protein/ml, E) or heart (0.05 mg of protein/mL, F) mitochondria were incubated in the presence of 5 mM succinate and 1 mM glutamate at the same as in A-D at 37 °C. Zero time corresponds to the substrates' addition. Small aliquots were taken in time and complex I-specific NADH:Q₁ reductase activity was assayed as described in the Materials and Methods section. 100% NADH:Q₁ reductase activity corresponds to 0.17 ± 0.01 or $0.66 \pm 0.01 \mu\text{mol NADH} \times \text{min}^{-1} \times \text{mg protein}^{-1}$ for the brain and heart enzyme, respectively. Results are mean \pm SD (n = 4).

4–5, ~1200 kDa and 850 kDa bands, respectively). A densitometric analysis of the bands' intensity showed a linear dependence of the band fluorescence intensity on the amount of loaded protein (Fig. 3B). The flavin fluorescence signal could be quantified by calibration with known amounts of flavin added directly on the gel surface during scanning. The threshold of flavin detection using the Typhoon instrument was estimated to be 15–40 fmol of FMN and the fluorescence intensity depended linearly on the amount of added FMN in the range of 0.5–10 pmoles (Fig. 3C). The calculated complex I content for intact brain and heart mitochondria was determined as 18.6 ± 1.0 and 39 ± 2 pmol/mg protein, respectively (see also Fig. 4 and Table 3).

3.3. FMN content of the brain and heart complex I after RET

Inactivation of complex I in brain mitochondria during RET in Fig. 2 has been shown to be due to the dissociation of the enzyme's natural cofactor FMN [18,26,35]. We analyzed flavin content of mitochondria oxidizing succinate, which has been associated with the drop of complex I activity in the brain but not in the heart preparation (Fig. 2E and F). The effect of 20 min incubation in RET-like conditions on FMN content of complex I and FAD content of α KGDHC in brain and heart mitochondria is shown in Fig. 4. Unlike heart mitochondria, complex I FMN content in the brain preparation was significantly decreased (Fig. 4B, left), indicating dissociation of FMN from its binding site when the respiratory chain is reduced by succinate in RET-like conditions. At the same time, FAD content of KGDHC did not change (Fig. 4B, right).

3.4. Kinetic analysis of the flavin-site reactions

In specific conditions, mitochondrial complex I can catalyze a number of reactions such as forward and reverse electron transfer [56, 57], transhydrogenase reaction [58,59], superoxide generation [60,61], and the kinetic patterns of reactions involving the FMN-binding site are far from being trivial. To further analyze any difference between brain and heart complex I, we examined the kinetic parameters of complex I NADH dehydrogenase reactions: physiological NADH oxidase (complexes I, III and IV together) and oxidation of NADH by artificial acceptor HAR, which reacts with the enzyme at or close to the FMN-binding site (Table 2). The effect of competitive inhibitors of the NADH binding site, such as ADP-ribose [23] and NAD⁺ [23,62,63], was also examined.

As expected, absolute NADH-dehydrogenase activities of complex I were higher in mitochondria from the heart than from the brain. No difference in K_m values for NADH and inhibition constants for the nucleotides in the physiological NADH oxidase reaction (complexes I, III and IV together) was found. However, in the NADH:HAR reductase reaction, brain complex I displayed a higher affinity for both oxidized and reduced nucleotides indicating a possible difference around the FMN-binding site between the brain and heart enzyme.

3.5. Catalytic turnover number of the heart and brain complex I

Although mitochondria from brain tissue differ in their enzymatic

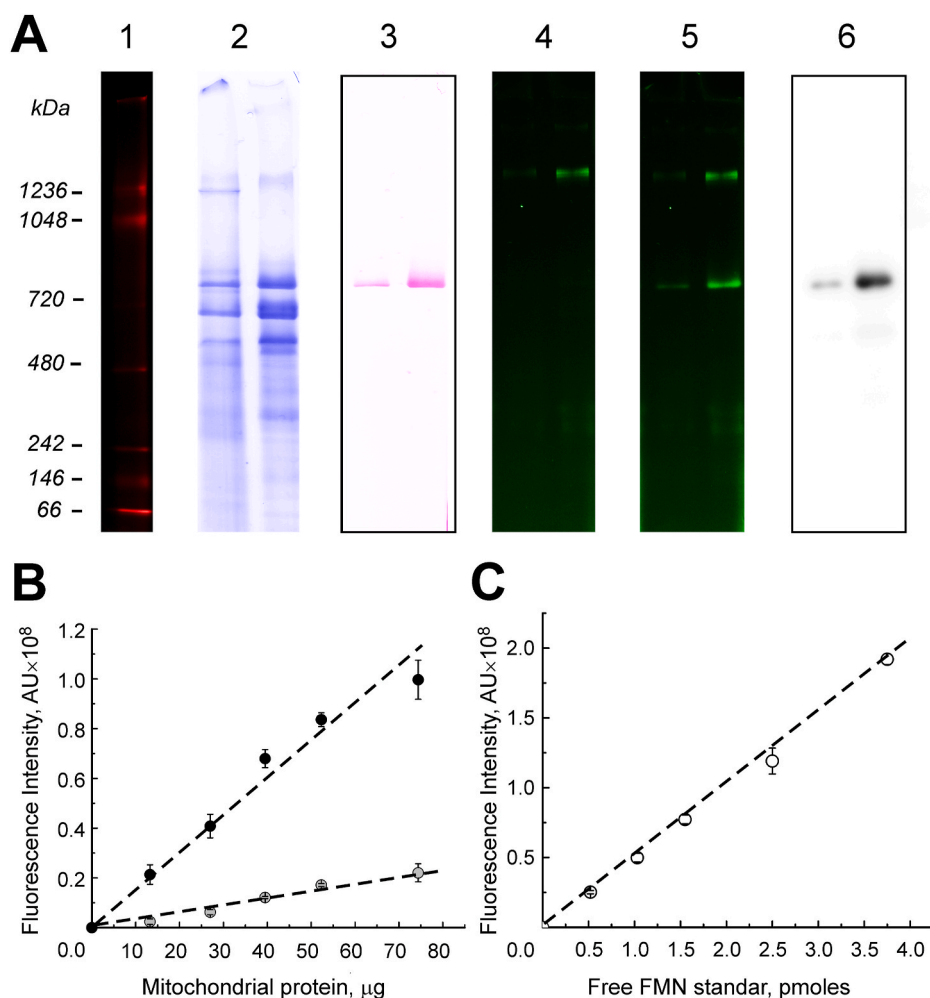


Fig. 3. Identification of Complex I FMN and FAD of α KGDHC in DDM-solubilized brain and heart mitochondria. (A) Intact mitochondria were solubilized using a DDM/protein ratio of 3.6 g/g. Identical aliquots of 15 μ g of total mitochondrial protein were loaded on an acrylamide gradient gel (3–12%). Heart (right) and brain (left) mitochondria samples were applied on the same gel and hrCN electrophoresis was performed as in Ref. [38]. Lanes 2, Coomassie stained gel strips showing the presence of complexes I–V with molecular weight markers (Lane 1); Lanes 3, complex I in gel activity strips; Lanes 4 and 5, flavin fluorescence from the same strip before (4) and after (5) treatment with 20% SDS (Excitation/Emission = 473/530 nm). Lanes 6, complex I immunodetection by Western blot using antibody against NDUFS8 subunit; (B) dependence of the flavin fluorescence intensity in the complex I (black circles) and α KGDHC (grey circles) bands upon protein load on the gel. Values are mean \pm SEM, n = 4; (C) calibration curve for flavin fluorescence signal made of standard free FMN solution applied directly on a gel and intensity of fluorescent spots measured (mean \pm SEM, n = 3).

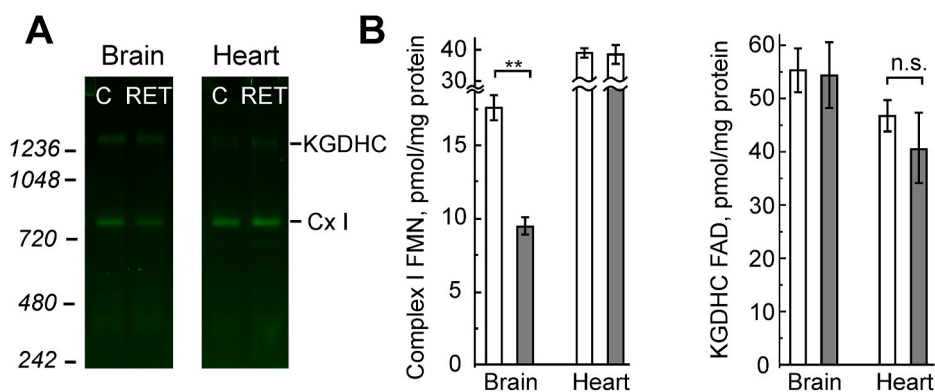


Fig. 4. Effect of succinate oxidation in RET-like conditions by preparations of brain and heart intact mitochondria on the content of mitochondrial flavins. Brain or heart mitochondria (0.2 and 0.25 mg/ml of protein respectively) were incubated for 20 min in conditions shown in Fig. 1. (A) Representative fluorescence image of an hrCN gel showing flavin signal from brain and heart mitochondria (25 and 10 μ g per well) before and after 20 min incubation in RET-like conditions; (B) Quantitative analysis of the content of complex I FMN (left) and FAD of α KGDHC (right) content in the brain and heart mitochondria at 0 and 20 min incubation in RET-like conditions (white and grey bars respectively). **p < 0.01, t-test, values are shown as mean \pm SEM. Three independent biological replicates were used for each experiment.

composition from heart mitochondria, the major quantitative differences are that cardiac preparations demonstrate higher respiration, ROS release and specific complex I activities per mg of protein due to a higher enzyme content (Fig. 4B, Table 3). Knowing complex I content of brain and heart mitochondria, we calculated enzyme turnover number (catalytic constant k_{cat} , min^{-1}) in NADH-dependent activities of both preparations using ubiquinone as a physiological and HAR as an artificial acceptor (Table 3). Both the HAR reductase turnover number and the ratio of HAR/Q turnover number were significantly higher in heart in comparison with brain membranes (Fig. 5).

3.6. Complex I subunit composition is different in the brain and heart

Why does cardiac complex I not lose its FMN after being reduced in RET-like conditions and why is the ratio of HAR/Q turnover different in the brain and heart enzyme? Our findings indicate that complex I might be structurally different in these tissues, and the difference is localized close to the FMN-binding site. This difference can be attributed to the subunit NDUFV3, which is the only known complex I subunit represented by two isoforms. The multi-exon-intron gene of NDUFV3 can be alternatively spliced, generating two protein isoforms from a single

Table 2

Relative affinities of nucleotides to heart and brain complex I in NADH oxidase and NADH:HAR reductase reactions.

	Brain	Heart
NADH-oxidase		
K_m^{NADH} (μM)	14 \pm 3	16 \pm 5
V_{max} ($\mu\text{mol NADH} \times \text{min}^{-1} \times \text{mg}^{-1}$)	0.7 \pm 0.13	2 \pm 0.44
$K_i^{NAD^+}$ (mM)	3.6 \pm 0.6	3 \pm 0.74
$K_i^{ADP-rib}$ (mM)	0.60 \pm 0.12	0.31 \pm 0.09
NADH:HAR		
K_m^{NADH} (μM)	60 \pm 7	102 \pm 13
$appK_m^{HAR}$ (mM)	0.52 \pm 0.10	0.94 \pm 0.10
V_{max} ($\mu\text{mol NADH} \times \text{min}^{-1} \times \text{mg}^{-1}$)	1.0 \pm 0.2	3.8 \pm 0.4
$K_i^{NAD^+}$ (mM)	9 \pm 6	17.4 \pm 4.0

Activities were assayed accordingly to the Materials and Methods section at 25 °C in 125 mM KCl, 0.2 mM EGTA, 20 mM HEPES-Tris (pH 7.4), 40 $\mu\text{g/ml}$ alamethicin and 1 mg/ml BSA in the presence of 1 mM HAR or 10 μM cytochrome c. 200 μM NADH was added to start the reaction. Values are given as mean \pm SD. Inhibition by ADP-ribose was assayed at pH 8.5.

Table 3

Complex I content and NADH-dependent activities in preparations of intact and DDM-solubilized brain and heart mitochondrial membranes.

Tissue	Complex I content (pmol/mg protein)	NADH:HAR ^a ($\mu\text{mol NADH} \times \text{min}^{-1} \times \text{mg}^{-1}$)		NADH:Q ₁ ($\mu\text{mol NADH} \times \text{min}^{-1} \times \text{mg}^{-1}$)	
		Intact membranes	DDM-solubilized	Intact membranes	DDM-solubilized
Brain	18.6 \pm 1.0	0.76 \pm 0.10	0.95 \pm 0.24	0.21 \pm 0.06	0.11 \pm 0.02
Heart	39 \pm 2	2.44 \pm 0.56	2.62 \pm 0.25	0.49 \pm 0.10	0.15 \pm 0.03

^a Activities were measured as described in the Materials and Methods section at 25 °C. 25 or 50 $\mu\text{g/ml}$ of brain or heart mitochondria, respectively, were added to the medium composed of 125 mM KCl, 0.2 mM EGTA, 20 mM HEPES-Tris (pH 7.4), 40 $\mu\text{g/ml}$ alamethicin, and 1 mg/ml BSA. The reaction was started by addition of 150 μM NADH. To obtain solubilized membranes, 500 μg of mitochondrial protein were solubilized using 3.6 g DDM/g protein. DDM-treated samples were centrifuged at 20,000 g for 20 min at 4 °C, and the supernatants were used for activities' determination. Values are given as mean \pm SD (n = 3).

gene: the short 10 kDa (NDUFV3-S) isoform found in most mouse tissues and the long 50 kDa variant found mostly in the brain and cultured cells (NDUFV3-L) [64–66] (Fig. 7A). Digestion of both isoforms results in the formation of unique peptides detectable by mass spectrometry allowing discrimination between them in mitochondria samples. We performed complexome profiling experiments using mouse brain and heart mitochondria from the C57BL6/J mouse strain used in this study (Supplementary Tables S1 and S2). The intensity signal for the corresponding isoforms was calculated in accordance to Ref. [40]. Analysis of peptide intensities (Fig. 6) revealed the presence of the short isoform in both tissues but a much higher abundance of the long isoform in the brain (1:3 ratio between the short and long isoform) (Fig. 6A). No peptides from the long isoform were found in the heart sample (Fig. 6B).

3.7. Long NDUFV3 subunit isoform of complex I may affect flavin binding in the brain enzyme

Due to the lack of a 3D structure for the long isoform of NDUFV3, we used homology modeling by the YASARA structure software package. Fig. 7A shows that NDUFV3-L shares its N and C-termini with the canonical NDUFV3-S isoform, but contains a large insertion in between. Homology modeling resulted in the structure of NDUFV3-L with a C-terminus that perfectly superimposes with previously identified short NDUFV3-S for the cardiac enzyme [45] (Fig. 7B). The C-terminus part, which is similar to the NDUFV3-S subunit, is followed by a flexible linker and then a structured N-terminus domain. This flexible linker of

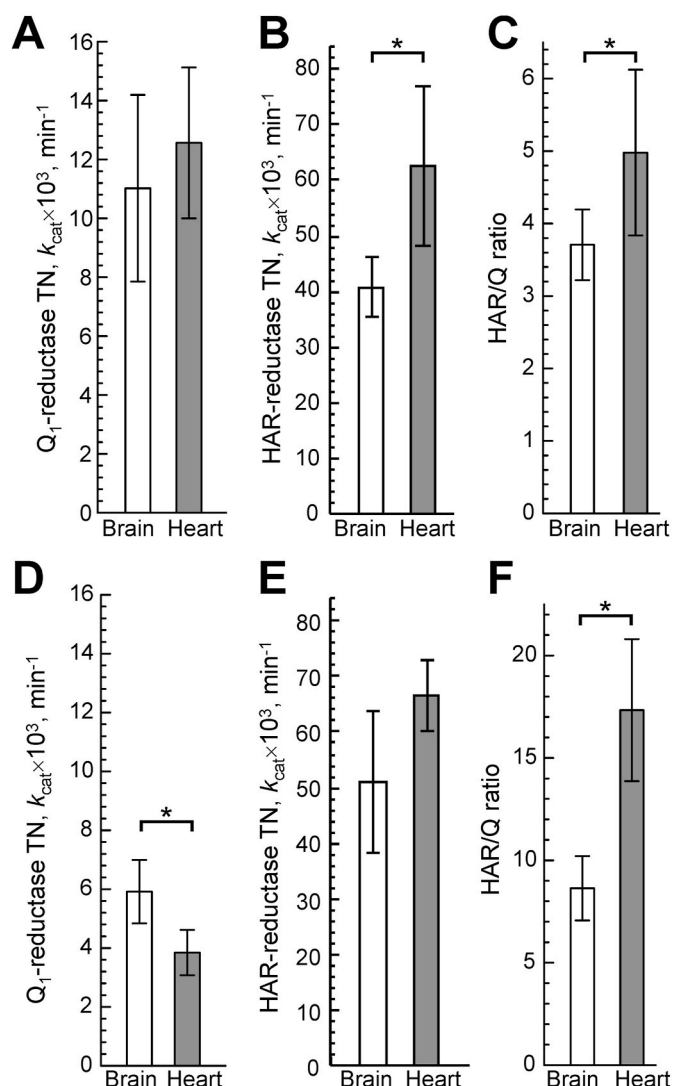


Fig. 5. Enzymatic turnover number (k_{cat}) of complex I in NADH-dependent reactions in brain and heart mitochondria. (A, B) represent the turnover number for NADH oxidation by Q₁ and artificial acceptor HAR, respectively, in intact mitochondrial fragments. Turnover number for solubilized membranes is shown in D and E. HAR/Q ratio in Complex I is higher in heart compared to brain as shown in C and F panels for total and solubilized membranes, respectively. Activities were measured accordingly to the Materials and Methods section. The values are shown as mean \pm SEM, n = 3.

NDUFV3-L permits the N domain to have a high degree of freedom and ability to directly bind to the subunits of the N-module of complex I. Using the ClusPro server for protein docking and the newly generated structure of NDUFV3-L, we found that the N-terminus domain of NDUFV3-L can interact with the FMN cavity of NDUFV1 (Fig. 7C). A similar interaction is impossible for the short NDUFV3-S because it is located on the opposite side of the complex I N-module and does not reach the FMN cavity.

4. Discussion

The major aim of this study was to quantitatively compare the recently characterized process of redox-dependent dissociation of FMN from complex I in mitochondria from the brain and heart. FMN is the first redox center of complex I that directly accepts electrons from the NADH molecule. The enzyme contains one molecule of flavin that is tightly but non-covalently bound to the 51 kDa (NDUFV1) subunit [67–73]. Electrons from the reduced flavin are transferred downstream

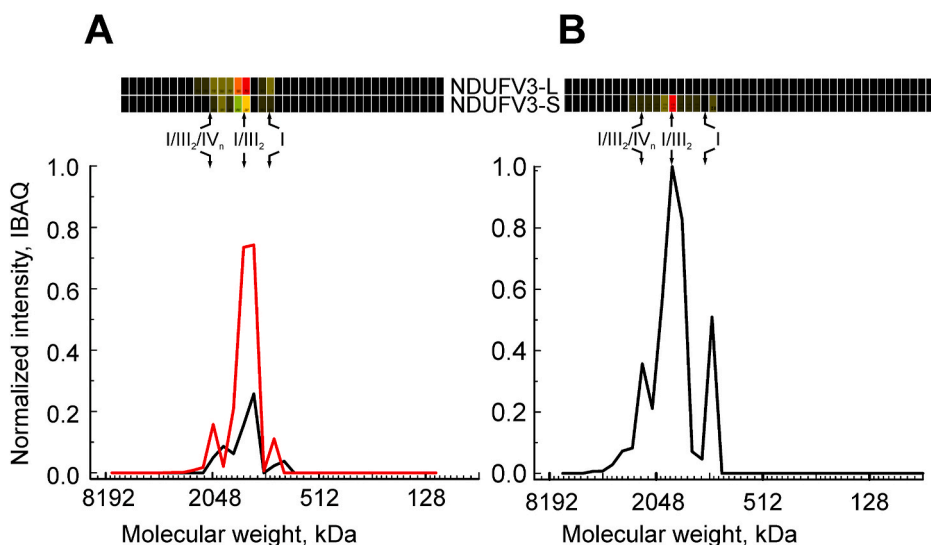


Fig. 6. Complexome profiling and mass spectrometric analysis of NDUFV3 isoforms in intact brain (A) and heart (B) mitochondria. Abundance of short and long NDUFV3 subunit isoforms (L and S, respectively) from cerebral and cardiac digitonin-solubilized mitochondria was normalized to maximal appearance and depicted in two heatmaps above the graphs. Assignment of complexes: I, complex I; I/III2, supercomplex containing complex I and dimer of complex III; I/III2/IVn, supercomplex containing complex I, dimer of complex III, and one to four copies of complex IV. Migration profiles showing the abundance of the unique peptides of NDUFV3 short (NDUFV3-S, isoform 2, black) and long (NDUFV3-L, isoform 1, red) isoforms in digitonin-solubilized mitochondria. (For interpretation of the references to colour in this figure legend, the reader is referred to the Web version of this article.)

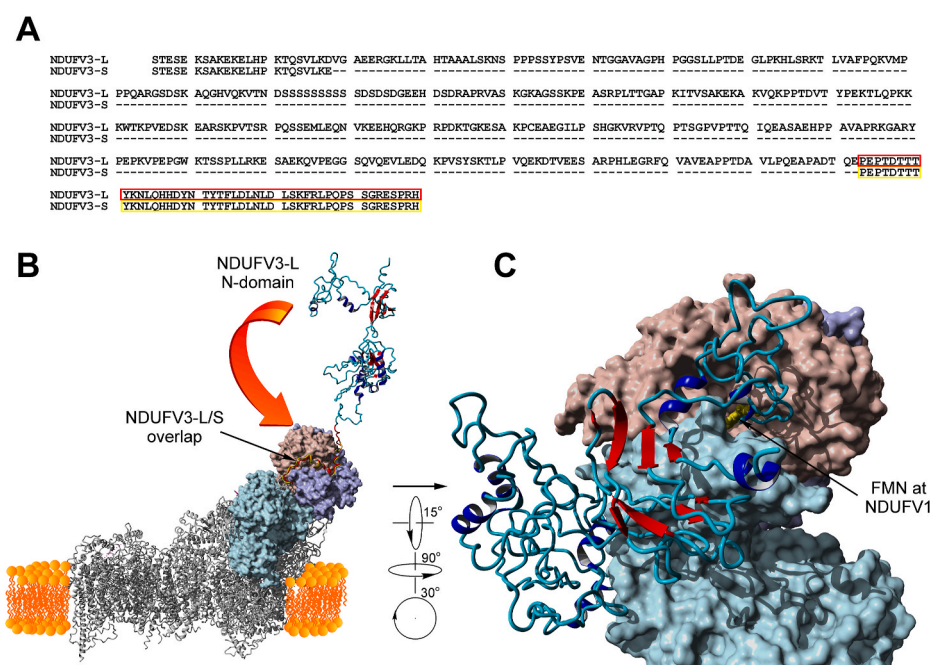


Fig. 7. Molecular docking of NDUFV3-L isoform at mitochondrial complex I. (A) Sequence alignment of the mature NDUFV-L and NDUFV-S isoforms with overlapping structures in the C-termini used for modeling are marked by red and yellow rectangles. (B) Tilted side view of mitochondrial complex I (PDB ID: 6G2J, [45]) showing molecular surfaces for three complex I N-module subunits (NDUFV1 is pale salmon, NDUFV2 is lavender, and NDUFV3 is teal). The superposition of overlapping structures at the C-terminus of NDUFV3-L (red) and NDUFV3-S (yellow) is shown as ribbons. The bending direction of the flexible linker of NDUFV3-L before the N-terminus domain is indicated by an orange arrow. Note that the cavity of the FMN binding site at NDUFV1 is on the other side of the complex I molecule. (C) Close-up view at the N-module (subunits NDUFS1, NDUFV1, NDUFS1 are shown as surfaces) with the FMN-binding cavity and ClusPro protein-protein docking arrangement of the NDUFV3-L N-domain (ribbons). The flexible linker adjoins along the surface of the N-module extending the NDUFV3-L N-domain close to the cavity containing a tightly bound FMN molecule (depicted in yellow within the pocket of NDUFV1). (For interpretation of the references to colour in this figure legend, the reader is referred to the Web version of this article.)

via the chain of FeS clusters to the final acceptor ubiquinone. Reduced flavin of complex I has also been proposed to be the main site of ROS-production in the respiratory chain ([60,61,74–76] see Ref. [77] for review). An enzyme that lacks FMN is not catalytically active and cannot react with pyridine nucleotides or participate in ROS generation [26,51,78]. FMN is bound at the bottom of a deep cavity of the NDUFV1 subunit [73,79] and is potentially accessible to molecular oxygen, so that reaction of oxygen with reduced or semireduced flavin generates ROS. However, due to spatial constraints, oxygen's accessibility to the reduced flavin is restricted if a substrate nucleotide is bound at the NDUFV1 subunit [74,79,80]. There are two ways to reduce FMN of the enzyme: directly by the substrate NADH (forward reaction) and in RET-like conditions as a potential-dependent reduction of the enzyme by ubiquinol (reverse reaction), both of which are discussed below.

From the thermodynamic analysis of bovine complex I [81], later confirmed by protein film voltammetry [82], it follows that reduced

FMNH₂ has more than four orders of magnitude lower affinity for its specific binding site than FMN. Here we showed that the kinetics of FMN dissociation during direct reduction by NADH in the forward reaction is very similar in mitochondria from the brain and heart. This fits well with earlier observations of the decrease in FMNH₂ affinity and its dissociation from bovine heart complex I and the homologous *E.coli* enzyme, indicating a highly conserved mechanism of cofactor dissociation when reduced by NADH [51–53]. As expected, exogenously added FMN recovered reduction-inactivated enzyme almost instantaneously due to the fast rate of FMN rebinding to the apoenzyme [51,53].

FMN can also be reduced in RET conditions, when electrons are supplied from ubiquinol via oxidation of succinate, and complexes III and IV provide a proton-motive force to drive electrons upstream. A dramatic difference in FMN dissociation kinetics between the brain and heart enzyme in RET-like conditions was observed using the H₂O₂ release as an indirect real-time measure for complex I activity as well as

assessing complex I activity directly. Using our novel approach for quantification of complex I FMN [39], we unambiguously demonstrated that, unlike in mitochondria from the heart, incubation in RET-like conditions decreases complex I FMN content in the brain enzyme. These observations suggest a difference in the vicinity of the complex I FMN-binding site between the brain and heart enzyme.

It should be stressed that in RET-like conditions, mitochondrial complex I produces ROS at a much higher rate than if the enzyme is reduced by NADH in the forward reaction [18,37,74,83]. This is due to the reoxidation of flavin by downstream FeS clusters before NAD⁺ is released [58], which limits the accessibility of reduced flavin to oxygen in the forward reaction. In RET-like conditions, on the other hand, no nucleotide is present at the narrow cavity when FMN is reduced “from the bottom”, so that oxygen reactivity toward flavin is not hindered, providing the highest rates of ROS generation. The restrictions applied by bound NADH/NAD⁺ during the forward reaction can explain the apparent lack of difference in the kinetics of FMN dissociation between the brain and heart enzyme when reduced by NADH. Bound NAD⁺ not only limits the oxygen accessibility to FMN but also could prevent dissociation of the reduced flavin from its binding site at NDUFV1. Therefore, the amount of flavin loss is defined by the rate of NAD⁺ dissociation and not by the structural features in the vicinity of the FMN-binding pocket. Another explanation is that the liberated FMNH₂ is quickly oxidized by oxygen [84,85] so that FMN may rebound to the apoprotein thus resulting in very slow cycling and apparent lack of difference between the brain and heart enzyme. The fate of matrix FMN during RET is less clear due to the presence of FMN-pyrophosphatase [86,87] that can convert released FMN to riboflavin, which cannot reactivate FMN-deficient enzyme [51,53].

Surprisingly, the enzyme kinetic parameters of complex I NADH dehydrogenase reactions and effect of inhibitors were very similar for both tissues, except an almost two-fold lower K_m for artificial acceptor HAR in NADH:HAR reductase catalyzed by the brain enzyme. In addition, the brain enzyme was found to be less sensitive to ADP-ribose, a competitive inhibitor of NADH oxidation. Our method for determination of absolute content of complex I in the brain and heart [39] allowed us to accurately estimate content and therefore catalytic turnover number for the physiological NADH:Q reaction and oxidation of NADH by HAR. We demonstrated that in intact membranes, heart complex I has a higher turnover number for the NADH:HAR reaction than the brain enzyme. Most likely HAR accepts electrons from the reduced or semireduced flavin via nucleotide [58], which further suggests a possible difference between the brain and heart enzyme around the FMN-binding site. In addition, the ratio of HAR/Q turnover number was greater in the heart in comparison with brain mitochondria, which also indicates intrinsic differences around the FMN-binding pocket in the heart and brain enzyme.

No significant change in the conformation of NADH-binding site of complex I upon reduction has been shown during catalytic turnover [88–91]. Therefore, it is very unlikely that FMN binding at the NDUFV1 subunit upon reduction of the enzyme (FMN and FeS clusters) is different in the brain and heart. At the same time, the reduced FMN molecule has two additional hydrogen atoms bound to nitrogen atoms 1 and 5 of the isoalloxazine ring. According to the high resolution structure of the mouse enzyme, this part of the nucleotide is not involved in any significant interaction with NDUFV1, and therefore the binding pocket itself is not changing upon reduction of the flavin [73,79,92,93]. At the same time, the change in geometry of the butterfly-like structure of the ring upon reduction [94,95] may contribute to the pronounced change in flavin affinity to its binding site. Therefore, redox-dependent interactions of NDUFV1 amino acid residues with its immediate ligand flavin are very likely to be the same in the brain and heart enzyme. Our quantitative results on redox-dependent FMN release from the enzyme are in good agreement with the published work from our laboratory [18, 26,39] and other groups [51,53]. It was of obvious interest to establish the reason for the functional differences of FMN-dependent reactions in

the brain and heart enzyme under RET-like conditions.

We propose that the difference in the kinetics of RET-induced reductive FMN dissociation is due to the presence of the recently identified long 50 kDa isoform of CxI subunit NDUFV3 (NDUFV3-L) [64–66]. The complexome profiling of mitochondria from C57BL/6J mice showed the presence of the NDUFV3-L isoform in brain mitochondria but not in the heart mitochondria, where only the short 10 kDa form was detected. Therefore, there is a solid structural basis for the observed functional difference between brain and heart complex I that has never been described before. It should be noted that preparation of intact brain mitochondria represents a mixture of the organelle from all brain cell types, such as neurons and glia. It is interesting that the abundance of the long isoform is threefold higher than the short one which is very similar to the neuron:glia total mass ratio in the mouse brain [96].

The short NDUFV3-S isoform is not fully resolved in the known structure of the mouse enzyme [45] but the C-terminus is located at the N-module of complex I on the opposite side of the FMN-binding cavity. Unlike the NDUFV3-S isoform, the N-terminus of the long brain-specific NDUFV3-L can be extended along the enzyme surface toward the FMN binding pocket and affect the nucleotide affinity to the apoenzyme. Our prediction suggests that brain NDUFV3-L, but not heart NDUFV3-S, can affect FMN binding to NDUFV1. Our modeling is highly suggestive of this possibility, and the exact mechanism of the NDUFV3-L alteration of FMN binding/unbinding to complex I in brain mitochondria can be defined after the structure of the brain enzyme is resolved.

5. Conclusion

We studied the effect of RET on mitochondrial complex I flavin dissociation in heart and brain mitochondria. Comparison of redox-dependent complex I flavin loss kinetics demonstrates that the dynamics of mitochondrial injury may significantly differ in both tissues. Our results suggest that different therapeutic strategies and resuscitation protocols should be used to alleviate mitochondrial injury during I/R in cases of stroke, heart infarction, or prolonged cardiac arrest.

Declaration of competing interest

The authors declare that they have no known competing financial interests or personal relationships that could have appeared to influence the work reported in this paper.

Acknowledgments

This work was partially supported by the grants NIH RO1NS112381 (A.G.), NS100850 (V.T.), R01HL132918 (R.R.), R01HL151447 (R.R.), AHA Postdoctoral fellowship 834220 (J.J.) and by the Deutsche Forschungsgemeinschaft: SFB815/Z1 (I.W.) and by BMBF mitoNET-German Network for Mitochondrial Disorders 01GM1906D (I.W.). We are grateful to Dr. Inna Krieger for critical reading of the manuscript. We thank Prof. Eric Green, Department of Biochemistry and Molecular Biophysics Columbia University Medical Center for access to the Typhoon instrument.

Appendix A. Supplementary data

Supplementary data to this article can be found online at <https://doi.org/10.1016/j.redox.2022.102258>.

References

- [1] S.S. Virani, A. Alonso, H.J. Aparicio, E.J. Benjamin, M.S. Bittencourt, C. W. Callaway, A.P. Carson, A.M. Chamberlain, S. Cheng, F.N. Delling, M.S.V. Elkind, K.R. Evenson, J.F. Ferguson, D.K. Gupta, S.S. Khan, B.M. Kissela, K.L. Knutson, C. D. Lee, T.T. Lewis, J. Liu, M.S. Loop, P.L. Lutsey, J. Ma, J. Mackey, S.S. Martin, D. B. Matchar, M.E. Mussolino, S.D. Navaneethan, A.M. Perak, G.A. Roth, Z. Samad, G.M. Satou, E.B. Schroeder, S.H. Shah, C.M. Shay, A. Stokes, L.B. VanWagner, N.

- Y. Wang, C.W. Tsao, E. American Heart Association Council on, C. Prevention Statistics, S. Stroke Statistics, Heart disease and stroke statistics-2021 update: a report from the American heart association, *Circulation* 143 (2021) e254–e743.
- [2] Q. Chen, S. Moghaddas, C.L. Hoppel, E.J. Lesnesky, Ischemic defects in the electron transport chain increase the production of reactive oxygen species from isolated rat heart mitochondria, *Am. J. Physiol. Cell Physiol.* 294 (2008) C460–C466.
- [3] Q. Chen, S. Moghaddas, C.L. Hoppel, E.J. Lesnesky, Reversible blockade of electron transport during ischemia protects mitochondria and decreases myocardial injury following reperfusion, *J. Pharmacol. Exp. Therapeut.* 319 (2006) 1405–1412.
- [4] S. Rehnroona, L. Mela, B.K. Siesjo, Recovery of brain mitochondrial function in the rat after complete and incomplete cerebral ischemia, *Stroke* 10 (1979) 437–446.
- [5] A. Galkin, Brain ischemia/reperfusion injury and mitochondrial complex I damage, *Biochemistry (Mosc.)* 84 (2019) 1411–1423.
- [6] H.A. Krebs, Intermediate metabolism of carbohydrates, *Nature* 138 (1936) 288–289.
- [7] H. Weil-Malherbe, Studies on brain metabolism: the metabolism of glutamic acid in brain, *Biochem. J.* 30 (1936) 665–676.
- [8] H. Weil-Malherbe, Studies on brain metabolism: formation of succinic acid, *Biochem. J.* 31 (1937) 299–312.
- [9] G. Benzi, E. Arrigoni, F. Marzatico, R.F. Villa, Influence of some biological pyrimidines on the succinate cycle during and after cerebral ischemia, *Biochem. Pharmacol.* 28 (1979) 2545–2550.
- [10] O. Pisarenko, I. Studneva, V. Khlopov, E. Solomatina, E. Ruuge, An assessment of anaerobic metabolism during ischemia and reperfusion in isolated Guinea pig heart, *Biochim. Biophys. Acta* 934 (1988) 55–63.
- [11] E.T. Chouchani, V.R. Pell, E. Gaude, D. Aksentijevic, S.Y. Sundier, E.L. Robb, A. Logan, S.M. Nadtochiy, E.N. Ord, A.C. Smith, F. Eyassu, R. Shirley, C.H. Hu, A. J. Dare, A.M. James, S. Rogatti, R.C. Hartley, S. Eaton, A.S. Costa, P.S. Brookes, S. M. Davidson, M.R. Duchon, K. Saeb-Parsy, M.J. Shattock, A.J. Robinson, L. M. Work, C. Frezza, T. Krieg, M.P. Murphy, Ischaemic accumulation of succinate controls reperfusion injury through mitochondrial ROS, *Nature* 515 (2014) 431–435.
- [12] P.V. Sahni, J. Zhang, S. Sosunov, A. Galkin, Z. Niatsetskaya, A. Starkov, P. S. Brookes, V.S. Ten, Krebs cycle metabolites and preferential succinate oxidation following neonatal hypoxic-ischemic brain injury in mice, *Pediatr. Res.* 83 (2017) 491–497.
- [13] J. Zhang, Y.T. Wang, J.H. Miller, M.M. Day, J.C. Munger, P.S. Brookes, Accumulation of succinate in cardiac ischemia primarily occurs via canonical krebs cycle activity, *Cell Rep.* 23 (2018) 2617–2628.
- [14] J.L. Martin, A.S.H. Costa, A.V. Gruszczak, T.E. Beach, F.M. Allen, H.A. Prag, E. C. Hinchy, K. Mahbubani, M. Hamed, L. Tronci, E. Nikitopoulou, A.M. James, T. Krieg, A.J. Robinson, M.M. Huang, S.T. Caldwell, A. Logan, L. Pala, R.C. Hartley, C. Frezza, K. Saeb-Parsy, M.P. Murphy, Succinate accumulation drives ischaemia-reperfusion injury during organ transplantation, *Nat. Metabol.* 1 (2019) 966–974.
- [15] Y. Zhang, M. Zhang, W. Zhu, J. Yu, Q. Wang, J. Zhang, Y. Cui, X. Pan, X. Gao, H. Sun, Succinate accumulation induces mitochondrial reactive oxygen species generation and promotes status epilepticus in the kainic acid rat model, *Redox Biol.* 28 (2020) 101365.
- [16] J. Kamarauskaite, R. Baniene, D. Trumbeckas, A. Strazdauskas, S. Trumbeckaite, Increased succinate accumulation induces ROS generation in *in vivo* ischemia/reperfusion-affected rat kidney mitochondria, *BioMed Res. Int.* 2020 (2020) 885585.
- [17] Z.V. Niatsetskaya, S.A. Sosunov, D. Matsiukevich, I.V. Utkina-Sosunova, V. I. Ratner, A.A. Starkov, V.S. Ten, The oxygen free radicals originating from mitochondrial complex I contribute to oxidative brain injury following hypoxia-ischemia in neonatal mice, *J. Neurosci.* 32 (2012) 3235–3244.
- [18] A. Stepanova, S. Sosunov, Z. Niatsetskaya, C. Konrad, A.A. Starkov, G. Manfredi, I. Wittig, V. Ten, A. Galkin, Redox-dependent Loss of Flavin by Mitochondrial Complex I in Brain Ischemia/reperfusion Injury, *Antioxid Redox Signal*, 2019.
- [19] B. Chance, G. Hollunger, Energy-linked reduction of mitochondrial pyridine nucleotide, *Nature* 185 (1960) 666–672.
- [20] P.C. Hinkle, R.A. Butow, E. Racker, B. Chance, Partial resolution of the enzymes catalyzing oxidative phosphorylation. XV. Reverse electron transfer in the flavin-cytochrome beta region of the respiratory chain of beef heart submitochondrial particles, *J. Biol. Chem.* 242 (1967) 5169–5173.
- [21] M. Klingenberg, W. Slenczka, [Pyridine nucleotide in liver mitochondria. An analysis of their redox relationships], *Biochem. Z.* 331 (1959) 486–517.
- [22] A.B. Kotlyar, A.D. Vinogradov, Slow active/inactive transition of the mitochondrial NADH-ubiquinone reductase, *Biochim. Biophys. Acta* 1019 (1990) 151–158.
- [23] T.V. Zharova, A.D. Vinogradov, A competitive inhibition of the mitochondrial NADH-ubiquinone oxidoreductase (Complex I) by ADP-ribose, *Biochim. Biophys. Acta* 1320 (1997) 256–264.
- [24] A. Heinen, M. Aldakkak, D.F. Stowe, S.S. Rhodes, M.L. Riess, S.G. Varadarajan, A. K. Camara, Reverse electron flow-induced ROS production is attenuated by activation of mitochondrial Ca²⁺-sensitive K⁺ channels, *Am. J. Physiol. Heart Circ. Physiol.* 293 (2007) H1400–H1407.
- [25] A.B. Kotlyar, N. Borovok, NADH oxidation and NAD⁺ reduction catalysed by tightly coupled inside-out vesicles from *Paracoccus denitrificans*, *Eur. J. Biochem.* 269 (2002) 4020–4024.
- [26] A. Stepanova, A. Kahl, C. Konrad, V. Ten, A.S. Starkov, A. Galkin, Reverse electron transfer results in a loss of flavin from mitochondrial complex I: potential mechanism for brain ischemia reperfusion injury, *J. Cerebr. Blood Flow Metabol.* 37 (2017) 3649–3658.
- [27] C.L. Quinlan, I.V. Perevoschikova, R.L. Goncalves, M. Hey-Mogensen, M.D. Brand, The determination and analysis of site-specific rates of mitochondrial reactive oxygen species production, *Methods Enzymol.* 526 (2013) 189–217.
- [28] A. Stepanova, C. Konrad, G. Manfredi, R. Springett, V. Ten, A. Galkin, The dependence of brain mitochondria reactive oxygen species production on oxygen level is linear, except when inhibited by antimycin A, *J. Neurochem.* 148 (2018) 731–745.
- [29] A.Y. Andreyev, Y.E. Kushnareva, A.N. Murphy, A.A. Starkov, Mitochondrial ROS metabolism: 10 Years later, *Biochemistry (Mosc.)* 80 (2015) 517–531.
- [30] A.A. Starkov, Measurement of mitochondrial ROS production, *Methods Mol. Biol.* 648 (2010) 245–255.
- [31] A.A. Starkov, G. Fiskum, Regulation of brain mitochondrial H₂O₂ production by membrane potential and NAD(P)H redox state, *J. Neurochem.* 86 (2003) 1101–1107.
- [32] A. Guaras, E. Perales-Clemente, E. Calvo, R. Acin-Perez, M. Loureiro-Lopez, C. Pujol, I. Martinez-Carrasco, E. Nunez, F. Garcia-Marques, M.A. Rodriguez-Hernandez, A. Cortes, F. Diaz, A. Perez-Martos, C.T. Moraes, P. Fernandez-Silva, A. Trifunovic, P. Navas, J. Vazquez, J.A. Enriquez, The CoQH₂/CoQ ratio serves as a sensor of respiratory chain efficiency, *Cell Rep.* 15 (2016) 197–209.
- [33] F. Scialo, A. Sriram, D. Fernandez-Ayala, N. Gubina, M. Lohmus, G. Nelson, A. Logan, H.M. Cooper, P. Navas, J.A. Enriquez, M.P. Murphy, A. Sanz, Mitochondrial ROS produced via reverse electron transport extend animal lifespan, *Cell Metabol.* 23 (2016) 725–734.
- [34] J.O. Onukwufor, B.J. Berry, A.P. Wojtovich, Physiological implications of reactive oxygen species production by mitochondrial complex I reverse electron transport, *Antioxidants* (2019) 8.
- [35] A. Kahl, A. Stepanova, C. Konrad, C. Anderson, G. Manfredi, P. Zhou, C. Iadecola, A. Galkin, Critical role of flavin and glutathione in Complex I-mediated bioenergetic failure in brain ischemia/reperfusion injury, *Stroke* 49 (2018) 1223–1231.
- [36] I. Gostimskaya, A. Galkin, Preparation of highly coupled rat heart mitochondria, *J. Vis. Exp.* 43 (2010), <https://doi.org/10.3791/2202>.
- [37] A. Stepanova, A. Galkin, Measurement of mitochondrial H₂O₂ production under varying O₂ tensions, *Methods Cell Biol.* 155 (2020) 273–293.
- [38] I. Wittig, M. Karas, H. Schägger, High resolution clear native electrophoresis for integral functional assays and fluorescence studies of membrane protein complexes, *Mol. Cell. Proteomics* 6 (2007) 1215–1225.
- [39] F. Ansari, B. Yoval-Sanchez, Z. Niatsetskaya, S. Sosunov, A. Stepanova, C. Garcia, E. Owusu-Ansah, V. Ten, I. Wittig, A. Galkin, Quantification of NADH:ubiquinone oxidoreductase (complex I) content in biological samples, *J. Biol. Chem.* 297 (2021) 101204.
- [40] H. Giese, J. Ackermann, H. Heide, L. Bleier, S. Drose, I. Wittig, U. Brandt, I. Koch, NOVA: a software to analyze complexome profiling data, *Bioinformatics* 31 (2015) 440–451.
- [41] H. Venselaar, R.P. Joosten, B. Vroiling, C.A. Baakman, M.L. Hekkelman, E. Krieger, G. Vriend, Homology modelling and spectroscopy, a never-ending love story, *Eur. Biophys. J.* 39 (2010) 551–563.
- [42] D. Kampjut, L.A. Sazanov, The coupling mechanism of mammalian respiratory complex I, *Science* (2020) 370.
- [43] A.M. Anger, J.P. Armache, O. Berninghausen, M. Habeck, M. Subklewe, D. N. Wilson, R. Beckmann, Structures of the human and *Drosophila* 80S ribosome, *Nature* 497 (2013) 80–85.
- [44] T. Yoshida, A. Yamagata, A. Imai, J. Kim, H. Izumi, S. Nakashima, T. Shiroshima, A. Maeda, S. Iwasawa-Okamoto, K. Azechi, F. Osaka, T. Saitoh, K. Maenaka, T. Shimada, Y. Fukata, M. Fukata, J. Matsumoto, H. Nishijo, K. Takao, S. Tanaka, S. Okabe, K. Tabuchi, T. Uemura, M. Mishina, H. Mori, S. Fukai, Canonical versus non-canonical transsynaptic signaling of neuronal 3 tunes development of sociality in mice, *Nat. Commun.* 12 (2021) 1848.
- [45] A.A. Agip, J.N. Blaza, H.R. Bridges, C. Viscomi, S. Rawson, S.P. Muench, J. Hirst, Cryo-EM structures of complex I from mouse heart mitochondria in two biochemically defined states, *Nat. Struct. Mol. Biol.* 25 (2018) 548–556.
- [46] D. Kozakov, D.R. Hall, B. Xia, K.A. Porter, D. Padhorny, C. Yueh, D. Beglov, S. Vajda, The ClusPro web server for protein-protein docking, *Nat. Protoc.* 12 (2017) 255–278.
- [47] D. Kozakov, R. Brenke, S.R. Comeau, S. Vajda, PIPER: an FFT-based protein docking program with pairwise potentials, *Proteins* 65 (2006) 392–406.
- [48] I.T. Desta, K.A. Porter, B. Xia, D. Kozakov, S. Vajda, Performance and its limits in rigid body protein-protein docking, *Structure* 28 (2020) 1071–1081 e1073.
- [49] S. Vajda, C. Yueh, D. Beglov, T. Bohnuud, S.E. Mottarella, B. Xia, D.R. Hall, D. Kozakov, New additions to the ClusPro server motivated by CAPRI, *Proteins* 85 (2017) 435–444.
- [50] D. Kozakov, D. Beglov, T. Bohnuud, S.E. Mottarella, B. Xia, D.R. Hall, S. Vajda, How good is automated protein docking? *Proteins* 81 (2013) 2159–2166.
- [51] P.J. Holt, R.G. Efremov, E. Nakamaru-Ogiso, L.A. Sazanov, Reversible FMN dissociation from *Escherichia coli* respiratory complex I, *Biochim. Biophys. Acta* 1857 (2016) 1777–1785.
- [52] V.D. Sled, A.D. Vinogradov, Reductive inactivation of the mitochondrial three subunit NADH dehydrogenase, *Biochim. Biophys. Acta* 1143 (1993) 199–203.
- [53] I.S. Gostimskaya, V.G. Grivennikova, G. Cecchini, A.D. Vinogradov, Reversible dissociation of flavin mononucleotide from the mammalian membrane-bound NADH: ubiquinone oxidoreductase (complex I), *FEBS Lett.* 581 (2007) 5803–5806.
- [54] W.S. Kunz, F.N. Gellerich, Quantification of the content of fluorescent flavoproteins in mitochondria from liver, kidney cortex, skeletal muscle, and brain, *Biochem. Med. Biol.* 50 (1993) 103–110.

- [55] W.S. Kunz, W. Kunz, Contribution of different enzymes to flavoprotein fluorescence of isolated rat liver mitochondria, *Biochim. Biophys. Acta* 841 (1985) 237–246.
- [56] A.D. Vinogradov, Catalytic properties of the mitochondrial NADH-ubiquinone oxidoreductase (Complex I) and the pseudo-reversible active/inactive enzyme transition, *Biochim. Biophys. Acta* 1364 (1998) 169–185.
- [57] V.G. Grivennikova, A.B. Kotlyar, J.S. Karliner, G. Cecchini, A.D. Vinogradov, Redox-dependent change of nucleotide affinity to the active site of the mammalian complex I, *Biochemistry* 46 (2007) 10971–10978.
- [58] J.A. Birrell, G. Yakovlev, J. Hirst, Reactions of the flavin mononucleotide in complex I: a combined mechanism describes NADH oxidation coupled to the reduction of APAD⁺, ferricyanide, or molecular oxygen, *Biochemistry* 48 (2009) 12005–12013.
- [59] G. Yakovlev, J. Hirst, Transhydrogenation reactions catalyzed by mitochondrial NADH-ubiquinone oxidoreductase (Complex I), *Biochemistry* 46 (2007) 14250–14258.
- [60] L. Kussmaul, J. Hirst, The mechanism of superoxide production by NADH: ubiquinone oxidoreductase (complex I) from bovine heart mitochondria, *Proc. Natl. Acad. Sci. U.S.A.* 103 (2006) 7607–7612.
- [61] A. Galkin, U. Brandt, Superoxide radical formation by pure complex I (NADH: ubiquinone oxidoreductase) from *Yarrowia lipolytica*, *J. Biol. Chem.* 280 (2005) 30129–30135.
- [62] Y. Hatefi, K.E. Stempel, Isolation and enzymatic properties of the mitochondrial reduced diphosphopyridine nucleotide dehydrogenase, *J. Biol. Chem.* 244 (1969) 2530–2537.
- [63] N.V. Zakharova, T.V. Zharova, A.D. Vinogradov, Kinetics of transhydrogenase reaction catalyzed by the mitochondrial NADH-ubiquinone oxidoreductase (Complex I) imply more than one catalytic nucleotide-binding sites, *FEBS Lett.* 444 (1999) 211–216.
- [64] H.R. Bridges, K. Mohammed, M.E. Harbour, J. Hirst, Subunit NDUFV3 is present in two distinct isoforms in mammalian complex I, *Biochim. Biophys. Acta Bioenerg.* 1858 (2017) 197–207.
- [65] S. Guerrero-Castillo, A. Cabrera-Orefice, M.A. Huynen, S. Arnold, Identification and evolutionary analysis of tissue-specific isoforms of mitochondrial complex I subunit NDUFV3, *Biochim. Biophys. Acta Bioenerg.* 1858 (2017) 208–217.
- [66] M.G. Dibley, M.T. Ryan, D.A. Stroud, A novel isoform of the human mitochondrial complex I subunit NDUFV3, *FEBS Lett.* 591 (2017) 109–117.
- [67] Y. Hatefi, J.S. Rieske, Preparation and properties of DPNH-coenzyme Q reductase (Complex I of the respiratory chain), *Methods Enzymol.* 10 (1967) 235–239.
- [68] C.I. Ragan, The structure and subunit composition of the particulate NADH-ubiquinone reductase of bovine heart mitochondria, *Biochem. J.* 154 (1976) 295–305.
- [69] N. Rao, S.P. Felton, F.M. Huennekens, Quantitative determination of mitochondrial flavins, in: *Methods Enzymol.*, Academic Press, 1967, pp. 494–499.
- [70] G. Belogradov, Y. Hatefi, Catalytic sector of complex I (NADH:Ubiquinone oxidoreductase): subunit stoichiometry and substrate-induced conformation changes, *Biochemistry* 33 (1994) 4571–4576.
- [71] L.A. Sazanov, P. Hinchliffe, Structure of the hydrophilic domain of respiratory complex I from *thermus thermophilus*, *Science* 311 (2006) 1430–1436.
- [72] K.R. Vinothkumar, J. Zhu, J. Hirst, Architecture of mammalian respiratory complex I, *Nature* 515 (2014) 80–84.
- [73] K. Fiedorczuk, J.A. Letts, G. Degliesposti, K. Kaszuba, M. Skehel, L.A. Sazanov, Atomic structure of the entire mammalian mitochondrial complex I, *Nature* 537 (2016) 644–648.
- [74] V.G. Grivennikova, A.D. Vinogradov, Generation of superoxide by the mitochondrial complex I, *Biochim. Biophys. Acta* 1757 (2006) 553–561.
- [75] Y. Liu, G. Fiskum, D. Schubert, Generation of reactive oxygen species by the mitochondrial electron transport chain, *J. Neurochem.* 80 (2002) 780–787.
- [76] C.L. Quinlan, R.L. Goncalves, M. Hey-Mogensen, N. Yadava, V.I. Bunik, M. D. Brand, The 2-oxoacid dehydrogenase complexes in mitochondria can produce superoxide/hydrogen peroxide at much higher rates than complex I, *J. Biol. Chem.* 289 (2014) 8312–8325.
- [77] A.Y. Andreyev, Y.E. Kushnareva, A.A. Starkov, Mitochondrial metabolism of reactive oxygen species, *Biochemistry (Mosc.)* 70 (2005) 200–214.
- [78] W. Fecke, V.D. Sled, T. Ohnishi, H. Weiss, Disruption of the gene encoding the NADH-binding subunit of NADH: ubiquinone oxidoreductase in *Neurospora crassa*. Formation of a partially assembled enzyme without FMN and the iron-sulphur cluster N-3, *Eur. J. Biochem.* 220 (1994) 551–558.
- [79] F. Varghese, E. Atcheson, H.R. Bridges, J. Hirst, Characterization of clinically identified mutations in NDUFV1, the flavin-binding subunit of respiratory complex I, using a yeast model system, *Hum. Mol. Genet.* 24 (2015) 6350–6360.
- [80] A.V. Kareyeva, V.G. Grivennikova, A.D. Vinogradov, Mitochondrial hydrogen peroxide production as determined by the pyridine nucleotide pool and its redox state, *Biochim. Biophys. Acta* 1817 (2012) 1879–1885.
- [81] V.D. Sled, N.I. Rudnitsky, Y. Hatefi, T. Ohnishi, Thermodynamic analysis of flavin in mitochondrial NADH: ubiquinone oxidoreductase (complex I), *Biochemistry* 33 (1994) 10069–10075.
- [82] C.D. Barker, T. Reda, J. Hirst, The flavoprotein subcomplex of complex I (NADH: ubiquinone oxidoreductase) from bovine heart mitochondria: insights into the mechanisms of NADH oxidation and NAD⁺ reduction from protein film voltammetry, *Biochemistry* 46 (2007) 3454–3464.
- [83] E.L. Robb, A.R. Hall, T.A. Prime, S. Eaton, M. Szibor, C. Viscomi, A.M. James, M. P. Murphy, Control of mitochondrial superoxide production by reverse electron transport at complex I, *J. Biol. Chem.* 293 (2018) 9869–9879.
- [84] V. Massey, Activation of molecular oxygen by flavins and flavoproteins, *J. Biol. Chem.* 269 (1994) 22459–22462.
- [85] Q.H. Gibson, V. Massey, N.M. Atherton, The nature of compounds present in mixtures of oxidized and reduced flavin mononucleotides, *Biochem. J.* 85 (1962) 369–383.
- [86] M. Barile, C. Brizio, D. Valenti, C. De Virgilio, S. Passarella, The riboflavin/FAD cycle in rat liver mitochondria, *Eur. J. Biochem.* 267 (2000) 4888–4900.
- [87] M. Barile, S. Passarella, A. Bertoldi, E. Quagliariello, Flavin adenine dinucleotide synthesis in isolated rat liver mitochondria caused by imported flavin mononucleotide, *Arch. Biochem. Biophys.* 305 (1993) 442–447.
- [88] J.M. Berrisford, L.A. Sazanov, Structural basis for the mechanism of respiratory complex I, *J. Biol. Chem.* 284 (2009) 29773–29783.
- [89] J.M. Berrisford, C.J. Thompson, L.A. Sazanov, Chemical and NADH-induced, ROS-dependent, cross-linking between subunits of complex I from *Escherichia coli* and *Thermus thermophilus*, *Biochemistry* 47 (2008) 10262–10270.
- [90] T. Friedrich, P. Hellwig, Redox-induced conformational changes within the *Escherichia coli* NADH ubiquinone oxidoreductase (complex I): an analysis by mutagenesis and FT-IR spectroscopy, *Biochim. Biophys. Acta* 1797 (2010) 659–663.
- [91] A.A. Mamedova, P.J. Holt, J. Carroll, L.A. Sazanov, Substrate-induced conformational change in bacterial complex I, *J. Biol. Chem.* 279 (2004) 23830–23836.
- [92] H.R. Bridges, J.G. Fedor, J.N. Blaza, A. Di Luca, A. Jussupow, O.D. Jarman, J. J. Wright, A.A. Agip, A.P. Gamiz-Hernandez, M.M. Roessler, V.R.I. Kaila, J. Hirst, Structure of inhibitor-bound mammalian complex I, *Nat. Commun.* 11 (2020) 5261.
- [93] D.N. Grba, J. Hirst, Mitochondrial complex I structure reveals ordered water molecules for catalysis and proton translocation, *Nat. Struct. Mol. Biol.* 27 (2020) 892–900.
- [94] J.D. Walsh, A.-F. Miller, Flavin reduction potential tuning by substitution and bending, *J. Mol. Struct.: THEOCHEM* 623 (2003) 185–195.
- [95] P. Hemmerich, G. Nagelschneider, C. Veeger, Chemistry and molecular biology of flavins and flavoproteins, *FEBS Lett.* 8 (1970) 69–83.
- [96] S. Herculano-Houzel, B. Mota, R. Lent, Cellular scaling rules for rodent brains, *Proc. Natl. Acad. Sci. U. S. A.* 103 (2006) 12138–12143.